

2020-05-10

Exoskeleton dissolution with mechanoreceptor damage in larval Dungeness crab related to severity of present-day ocean acidification vertical gradients

Bednarsek, N

<http://hdl.handle.net/10026.1/16753>

10.1016/j.scitotenv.2020.136610

Science of The Total Environment

Elsevier BV

All content in PEARL is protected by copyright law. Author manuscripts are made available in accordance with publisher policies. Please cite only the published version using the details provided on the item record or document. In the absence of an open licence (e.g. Creative Commons), permissions for further reuse of content should be sought from the publisher or author.

Exoskeleton dissolution with mechanoreceptor damage in larval Dungeness crab related to severity of present-day ocean acidification vertical gradients

Authors: Nina Bednaršek¹, Richard A. Feely², Marcus W. Beck¹, Simone R. Alin², Samantha A. Siedlecki³, Piero Calosi⁴, Emily L. Norton⁵, Casey Saenger⁵, Jasna Štrus⁶, Dana Greeley², Nikolay P. Nezlin¹, Miranda Roethler¹, John I. Spicer⁷

Affiliations:

¹Southern California Coastal Water Research Project, Costa Mesa, CA, 92626 USA

²NOAA Pacific Marine Environmental Laboratory, 7600 Sand Point Way NE, Seattle, WA, 98115 USA

³Department of Marine Sciences, University of Connecticut, Groton, Connecticut 06340

⁴Département de Biologie, Chimie et Géographie, Université du Québec à Rimouski, 300 Allée des Ursulines, Rimouski, QC G5L 3A1, Canada

⁵Joint Institute for the Study of the Atmosphere and Ocean, University of Washington, Seattle, WA, 98195 USA

⁶Department of Biology, Biotechnical Faculty, University of Ljubljana, Ljubljana, Slovenia

⁷University of Plymouth, School of Biological and Marine Sciences, Plymouth PL4 8AA, UK

***Corresponding author:** Nina Bednaršek (ninab@sccwrp.org); (714) 755-3237

Running title: Dungeness crab sensitivity to acidification

Keywords: Dungeness crab, larval sensitivity, global climate change, ocean acidification, exoskeleton structure, dissolution, mechanoreceptor damage.

Abstract:

Ocean acidification (OA) along the US West Coast is intensifying faster than observed in the global ocean. This is particularly true in nearshore regions (< 200 m) that experience a lower buffering capacity while at the same time providing important habitats for ecologically and economically significant species. While the literature on the effects of OA from laboratory experiments is voluminous, there is little understanding of present-day OA *in-situ* effects on marine life. Dungeness crab (*Metacarcinus magister*) is perennially one of the most valuable commercial and recreational fisheries. We focused on establishing OA-related vulnerability of larval crustacean based on mineralogical and elemental carapace to external and internal carapace dissolution by using a combination of different methods ranging from scanning electron microscopy, energy dispersive X-ray spectroscopy, elemental mapping and X-ray diffraction. By integrating carapace features with the chemical observations and biogeochemical model hindcast, we identify the occurrence of external carapace dissolution related to the steepest Ω calcite gradients ($\Delta\Omega_{\text{cal},60}$) in the water column. Dissolution features are observed across the carapace, pereopods (legs), and around the calcified areas surrounding neuritic canals of mechanoreceptors. The carapace dissolution is the most extensive in the coastal habitats under prolonged (1-month) long exposure, as demonstrated by the use of the model hindcast. Such dissolution has a potential to destabilize mechanoreceptors with important sensory and behavioral functions, a pathway of sensitivity to OA. Carapace dissolution is negatively related to crab larval width, demonstrating a basis for energetic trade-offs. Using a retrospective prediction from a regression models, we estimate an 8.3% increase in external carapace dissolution over the last two decades and identified a set of affected OA-related sublethal pathways to inform future risk assessment studies of Dungeness crabs.

Introduction

Since the pre-industrial era, anthropogenic CO₂ uptake along the US West Coast have resulted in rapid intensification OA rate on a global scale (Chavez et al., 2017; Feely et al., 2016), resulting in lower carbonate conditions compared to the pre-industrial times. This is because of the low regional buffering capacity, which contributes to low pH and carbonate mineral saturation states for both aragonite (Ω_{ara}) and calcite (Ω_{cal}) (Feely et al., 2018). These changes in carbonate chemistry have resulted in substantially reduced habitat suitability for marine calcifiers (Bednaršek et al., 2014; Somero et al., 2015). These findings are supported by the field and synthesis work along the North American Pacific demonstrating that calcifying invertebrates will be the ones most impacted by progressive OA (Bednaršek et al., 2017; Busch & McElhany, 2016). Apart from evidence of OA impacts on pteropods and other calcifiers caused by the low Ω_{ara} conditions in upwelling systems (Bednaršek et al., 2014, 2017) and around CO₂ vent seeps and sites (Manno et al., 2019; Tunnicliffe et al., 2009), there is limited understanding of present-day OA effects on marine life *in situ*. That is especially relevant for the crustaceans since they were considered less sensitive to OA parameters (like pCO₂ or pH) after studies demonstrated their capacity to abate initial hypercapnia and to buffer extracellular acid-base disturbances (Melzner et al., 2009; Pane and Barry, 2007) with limited or no change in aerobic metabolism (Paganini et al., 2014). However, restoring internal pH to sustain physiological and biogeochemical processes (Somero, 1986), typically requires activation of buffering, which is energetically expensive process (Cameron, 1985; Michaelidis et al., 2005). Recent experimental findings have demonstrated increased sensitivity to OA-related stressors in crustaceans, especially in the early life stages that can be regarded as a potential bottleneck for the population level responses (Schiffer et al., 2014; Small et al., 2015). Regardless of the

habitats that different species inhabit, the studies investigating OA effect on larval stages reported lower growth and decreased survival of blue crab (Giltz and Taylor, 2017), delayed metamorphosis in the stone crab (Gravinese et al., 2018), changes in exoskeleton composition (Page et al., 2016) and decreased metabolisms in Tanner crabs (Long et al., 2016) and increased energetic costs in the porcelain crab (Carter et al., 2013), while the pre-larval of the Dungeness crab showed reduced survival and slower progression through the development (Miller et al., 2016). With annual revenues up to \$220 million (Hodgson et al., 2018; Pacific States Marine Fisheries Commission, 2019), the Dungeness crab (*Metacarcinus magister*) is one of the most valuable and recreational fisheries in the US coastal waters. Terminal stage of pelagic Dungeness crab larvae (megalopae) undergoes long distance transport along the north Pacific coast of North America before settling in suitable benthic settlement site (Shanks, 1995; Sinclair, 1988). Given their diel vertical migration extends down to 60 m depth (Hobbs et al., 1992), megalopae encounter steep vertical pH, Ω_{cal} gradients in coastal habitats; however, the duration and magnitude of their exposure to these conditions remains largely unknown despite the exposure history notably impacting organismal responses (*sensu* Bednaršek et al. (2017)).

To start addressing potential OA vulnerability of the pelagic Dungeness larvae *in situ*, their spatial distribution must be paired with *in situ* exposure history (as defined in Bednaršek et al., 2017), understanding of their physiological susceptibility and their structural and mineralogical features. In regards to the later, surprisingly little is known about these features that can predispose an individual to extensive exoskeleton dissolution if the conditions in the external environment are conducive for it. In addition, for detecting environmental clues, the decapod exoskeleton contains elongated hair-like structures called setae, which are important chemo- and mechanoreceptors involved in sensory and behavioral responses. While the

lipoproteic epicuticle-covered exoskeleton consists of two cuticular mineral carbonate layers (Chen et al., 2008) (i.e., the outer exocuticle and the inner endocuticle) in the Dungeness crab adults such structure or its composition is completely unknown for the larvae.

This interdisciplinary study integrates physical, geochemical, biological, and modelling components across the individual and population-level parameters. Identification of the carapace crystalline mineralogical and elemental composition provided an understanding behind the extensive exoskeleton dissolution and mechanoreceptor damage. The latter was linked with the chemical observations made along the North American West Coast to identify the drivers and OA hotspots of *in situ* megalopae vulnerability. The biogeochemical model hindcast was used to determine the impact of *in situ* exposure history in the coastal habitats.

Materials and methods

Carbonate chemistry, sampling and analyses

For the purpose of this study, the NOAA West Coast Ocean Acidification (WCOA) cruise in May–June 2016 sampled conductivity, temperature, depth, and oxygen. Data on the conductivity, temperature, and pressure of seawater (CTD) were collected along cross-shelf transects, accompanied by biological stations with vertical sections of temperature (T), salinity, nutrients, oxygen, chlorophyll-a (chl-a), dissolved inorganic carbon (DIC), total alkalinity (TA), spectrophotometric pH (measured at 25°C and corrected to *in situ* temperatures, and expressed on the total pH scale, subsequently expressed pH_T). *p*CO₂ and calcite saturation state (Ω_{cal}) were calculated using CO2SYS as described by Feely et al. (2016) and Bednaršek et al. (2012). Larvae were collected using Neuston and Bongo nets with a mesh size of 333 μm , which were deployed

in an oblique manner at 10 stations during the night in the upper surface waters, an area that encompasses the nocturnal vertical habitat of larval Dungeness crabs of the upper 60 m (Hobbs et al., 1992; Morgan, 1985), with the following environmental parameters along the vertical habitat (Table S1). The duration of tows was 15–20 min. Megalopae were identified and then stored in 100% non-denatured ethanol, and also flash-frozen at -80 °C for later comparison of two different preservation methods.

Using SEM methods to detect and evaluate carapace dissolution

Megalopae carapaces were investigated using a combination of different methods: 1) scanning electron microscopy (SEM; Hitachi Phenom, USA) to determine potential structural changes on the cuticular surface; 2) energy dispersive X-ray spectroscopy (EDXS at the University of Washington) for mineralogical composition; 3) elemental mapping; and X-ray diffraction (University of Washington and Max Planck Institute) for elemental content across mostly lipoproteic carapace (Figure S1, Fig. 1). Here, we define exoskeleton as the cuticle covering the dorsal part of the carapace of the larval crab, and five pereopods, with chelae. The carapace epicuticle, which otherwise overlies the crystalline layer and makes dissolution observations impossible, was removed from each megalopa prior to analysis. This was accomplished using sodium hypochlorite, which efficiently removes the epicuticle but does not damage the crystalline layers underneath, even at high concentrations (Bednaršek et al., 2012). On the samples with no hypochlorite treatment, the epicuticle covered the crystalline layer so no investigation of dissolution was possible. Therefore, we tested different concentrations and duration of hypochlorite treatment on the individuals from the same station to ensure that we fully removed the epicuticle, without triggering dissolution of the calcite crystalline layers beneath it. The combination of 1 and 3 % sodium hypochlorite with 15, 30, and 120 min

treatments only partially removed the epicuticle, , while 6% hypochlorite treatments for 4 and 6 hours were effective in epicuticle removal, without inducing additional dissolution at the longer duration.

To determine the treatment does not induce any damage, we have tested the individuals from the same stations with different combination of treatments. We assumed the similarity of exposure history of individuals within the same stations (see modelling section). The results of no difference in dissolution under the different combination of concentration/duration of treatment combination was a confirmation that the treatment did not induce any additional damage, and thus did not confound our field observations.

We determined 6% hypochlorite for 3-4 h to be an efficient and effective treatment, similar to the treatment previously described for the removal of the periostracum in pteropods (Bednaršek et al., 2012). After soaking in sodium hypochlorite, samples were rinsed several times in Millipore water to remove any organic matter remaining on the surface of the exoskeleton. It is important to note that when examining the presence of setae within the neuritic canals, we did not use any treatment in order to avoid any methodological artifacts. When examining the internal area of the cuticle, we avoided examining the proximity of the gills given that dissolution could be impacted by the processes around. To quantify the dissolution of internal carapace cuticle, the pereopods and soft tissue of larvae were gently removed from the rest of the body and washed in Millipore water to remove any remaining tissue or organics before treatment with sodium hypochlorite. Each of the five pereopod cuticle was examined across the proximal and distal ends, with particular focus on chelae (Figure S2). SEM was used to evaluate the extent and severity of dissolution. We focused on three distinct features: ridging structures, dissolution around setae, and exposed calcite crystals (Figure S2, S3).

For estimating the various body parameter change (in mm) of larvae across various vertical OA gradients, we have measured carapace length (CL), total length from rostrum to telson (TL), length from rostrum to dorsal carapace spine (R-DCS), and carapace width (CW). The CW is the most commonly used parameter by various US federal agencies along the US West Coast to regulate crab management catch efforts (Davis et al., 2017). Here, we assume that all the larvae were released at the same time to allow for body parameter comparisons across different stations. Using the methodology to characterize the megalopae stages by González-Gordillo et al. (2004), we determined that all megalopae were in the intermolt stage, except for those from Station 115, which were transitioning into the premolt stage. We excluded the results of the internal dissolution observations from this station in case promoting process changed any features on the internal side that could bias accurate dissolution assessment.

Semi-quantitative dissolution assessment

Altogether, we analyzed 50 individuals from 10 environmental stations across OA-related vertical gradients of varying strength. We used 3–5 individuals per station to determine dissolution extent of the external side of carapace cuticle, as well as the cuticle of the pereopods. We used an additional 2–3 individuals per station to analyze the internal side of the cuticle. Approximately 10–20 SEM images were produced per individual on the external and internal sides, with the images being manually examined to detect any signs of dissolution. For crystal exposure characterization, the same categorization of dissolution conditions as previously described in pteropods was used (Bednaršek et al., 2012). We identified three major features of exoskeleton dissolution and developed a categorization scheme for all three features, showing them in their intact forms (Stage 0, Figure S2) and progressively altered forms (Stage 1 and 2; Figure S1; Table S2). These features differentiated damaged surfaces from the intact surfaces

(Table S2). The cuticular surface of the carapace and the pereopods under high Ω_{cal} *in situ* conditions had a smooth, sleek appearance (Figure S2; Stage 0). At greater magnification, individual calcite crystals were visible in these areas (Figure S2). Signs of dissolution tended to be more prevalent and more severe on the surface immediately surrounding setae pores. Consequently, areas around the setae were considered separately from the rest of the exoskeleton. From these observations, a semi-quantitative scoring metric was developed based on previous work on pteropods and used to score the remainder of the samples. For each sample, the three separate features (presence and depth of ridge structures, exposure of individual calcite crystals, and the prevalence of dissolution features around setae pores) were each assigned a score. The features were scored on a scale of 0 to 1 based on the severity of dissolution: intact exoskeleton with no dissolution received a score of 0; moderate dissolution received a score of 0.5; and substantial dissolution of all examined features was scored 1 (Figures S1–S3). Since the crab exoskeleton of the carapace and pereopod differ in their chemical composition, these three areas were assigned separate scores. Because of the surface analyses required separately for the external and internal dissolution, both types of analyses could not be conducted on the same individual. All three features displayed similar trends, so the scores were averaged to unitless ‘relative dissolution’, describing internal and external dissolution. Observation of setae presence/absence was included in the exoskeleton observation under SEM on intact specimen before any preparation treatments were conducted to eliminate the possibility of preparation steps affecting setae presence or outrooting them from the carapace.

Mineralogical analyses

The mineralogy of selected megalopae was characterized using X-ray diffraction (D8 Discover 2D; University of Washington, Seattle). Prior to analysis, carapaces from five megalopae at each

site were coarsely crushed and treated for 10 min using a dilute (3%) sodium hypochlorite solution to minimize interference from organic matter but without compromising mineralized structures. Samples were dried completely and then ground to a fine homogenous powder representing the aggregate of the five individuals from each location. Resulting diffractograms were compared to a catalog of mineral-specific patterns to constrain the primary mineralogy of each sample.

Elemental analyses

We used energy-dispersive X-ray spectroscopy (EDXS) to estimate elemental composition of the carapace and pereopod cross-sections (N = 7) from samples across different natural OA vertical gradients over spatial scales. For elemental analyses, we have not removed the epicuticle from the samples. These gradients analyses were conducted at Max Planck Institute for Marine Microbiology in Bremen, Germany. Prior to analyses, we dehydrated samples using 100 % ethanol and dried them in a critical point dryer. We prepared the sections by fracturing different carapace regions which was followed by the EDXS investigations (Figure 1).

Statistical analyses

Biological measurements from Dungeness megalopae collected at 10 stations along the North American Pacific Coast (Figure 2) were paired with synoptic environmental data from CTD profiles. Environmental data were summarized as depth-integrated averages from the surface to the maximum depth of each CTD profile to characterize the exposure conditions in the upper water column. In addition, $\Delta\Omega_{\text{cal},60}$ was estimated as the difference from the observed measurement at each depth bin with that of the surface. This measurement characterized the relative Ω_{cal} gradients with increasing depth and accounted for differences in the relative

magnitudes of Ω_{cal} between stations. Chlorophyll-a observations were highly skewed and so were log-transformed prior to analysis.

Biological responses included dissolution, body parameter, and abundance with various environmental vertical gradients to identify significant associations using generalized linear models. For comparison of the biological data to environmental conditions, each depth bin for the depth-integrated values was evaluated to identify at which depth associations between biological response and selected environmental variables were strongest. In addition, carapace dissolution was compared to body parameters to characterize potential linkage between the physiological parameters, growth, and population-level effects (abundance). Comparisons of biological measures to each other were also accomplished with generalized linear models.

Gaussian distributions were assumed for all response variable models, excluding presence/absence, which was modeled using a binomial logistic response curve. Models and individual parameters were considered significant at $\alpha = 0.05$. All models had $N = 10$ except presence/absence models with $N = 24$, which included additional stations where tows were conducted but no crabs were found. Finally, all variables were evaluated together to identify pairwise associations using Pearson correlation analysis and redundancy analysis (RDA) to characterize how the biological response measures were jointly explained by the environmental variables. For the latter analysis, all input data were standardized to range from 0 to 1 to account for differences in scale between variables. The *vegan* package for the R statistical programming language was used for standardization and RDA (Oksanen et al., 2019; R Core Team, 2019).

For selected predictors, additional models were developed to evaluate the additive effects of two predictors on dissolution. Backward model selection was used to identify the most parsimonious model by sequentially dropping individual predictors and comparing Akaike

Information Criterion values (AIC) (Akaike, 1973; Fox and Weisberg, 2011). This allowed us to determine if there was any additional power in combining predictors to explain dissolution, or consequently, if dissolution could be sufficiently explained using only one predictor. For example, the ability of both Ω_{cal} and chlorophyll to explain dissolution were evaluated to better understand the relative effects of both.

J-SCOPE model outputs of the larval exposure history prior to sampling

The Joint Institute for the Study of the Atmosphere and Ocean (JISAO)'s Seasonal Coastal Ocean Prediction of the Ecosystem (J-SCOPE, <http://www.nanoos.org/products/j-scope/>) features dynamical downscaling of regional ocean conditions in Washington and Oregon waters (Siedlecki et al., 2016). Model performance and predictability examined for sea surface temperature (SST), bottom temperature, bottom O_2 , pH, and Ω_{ara} through model hindcast, reforecast, and forecast comparisons with observations, showing significant measurable skill on seasonal timescales (Kaplan et al. 2016; Siedlecki et al., 2016; Norton et al., *in revision*). Megalopae exposure histories were simulated by releasing 100 representative particles, with vertical migration behavior over 60 m inserted into the predicted circulation field at each of the *in situ* sampling locations and times, and then tracking them backward in time for 30 d following methods described for pteropods in Bednaršek et al. 2017, and for megalopae in Norton et al., *in revision*. The vertical migration behavior was simulated using the LTRANSv2b larval transport model (North et al., 2008, 2011; Schlag and North, 2012) that has recently been implemented in the J-SCOPE system and adapted for megalopae (Norton et al., *in revision*).

Results

Elemental and crystalline characterization of the carapace

The compilation of our results demonstrate that the carapace is highly mineralized and precipitated into a chitin-proteinaceous matrix. XRD identify calcite as a primary polymorph in the carapace. The mineralized exoskeleton of the megalopae intermolt stages consists of the thinner exocuticle on the surface that is less than 2–3 μm thick, and the thicker and more compact endocuticle underneath (Figure 1) of approximately 6–7 μm , with the combined thickness up to 10 μm . The carapace surface is extensively covered with setae that are rooted in the calcified neuritic canals each with an average of about 5 μm surface opening (Figures S2 and S3). EDXS investigations characterized detailed elemental structure with average Ca^{2+} content of 28 % in the carapace and pereopods, with much higher Ca^{2+} found within in the mid layer and the endocuticle (higher than 50%) compared to less than 20% found in the exocuticle (Figure 1). The carapace endocuticle contains also a high concentration of Mg^{2+} with some areas of the carapace exceeding 5% content, categorizing it as a more soluble high-Mg calcite. In addition, the internal side contain high concentrations of phosphorus (up to 6%) and strontium (up to 2%) on the inner endocuticle (Figure 1). The percentage of different dissolution features is similar between the carapace and the pereopods, however with much less variation in all elements between the carapace and pereopods (Figure S1). This elemental composition indicates that other crystalline forms of carbonate could be precipitated into a chitin-proteinaceous matrix, such as an amorphous calcium carbonate (ACC) crystalline layer, but the methods used were not suitable for ACC detection. The strong presence of autofluorescence prevented more precise detection of any other crystalline forms, despite extensive use of Raman spectroscopy for this purpose. Nevertheless, such elemental structure resembles a layer of ACC with Mg^{2+} , phosphate and

carbonate-rich phase, or ACC with magnesian calcite, as previously demonstrated in the edible crabs *Cancer pagurus* (Fabritius et al., 2012).

Megalopae habitat characterization with strong vertical and spatial Ω_{cal} vertical gradients

Crab megalopae were found in both outer-shelf, slope, as well as nearshore (<200 m depth) habitats, with distinctly different vertical environmental gradients in the upper water column. Due to the upwelling of deeper, colder, CO₂-rich waters in the near-shore and coastal habitats, steep gradients in low pH and Ω_{cal} values were observed. In comparison, offshore region were characterised with more uniform vertical gradients with lower vertical difference over the same depth interval (Figure 2). Pronounced steep OA-related vertical habitats were observed in the upper 60 m of the water column, here represented as the difference between the surface and 60 m depth ($\Delta\Omega_{cal,60}$ or ΔpH_{60}), which is within the lower range of megalopae diel vertical migration habitat. Among all tested depths, statistical models comparing biological responses (e.g. exoskeleton dissolution, body parameters, abundance) with environmental conditions had the strongest associations using the 60 m vertical depth integrated value (e.g., external dissolution on body parts vs. $\Delta\Omega_{cal}$ had the highest $R^2 = 0.821$ at 60 m). Hereafter, all environmental data are reported using the 60 m depth integrated values. Coastal conditions recorded near-saturation Ω_{cal} values down to 1.4, pH down to 7.48, and pCO₂ up to 910 uatm (Table S1; Figure 2).. There were no observations of $\Omega_{cal} < 1$ or hypoxia, with similar oxygen ranges observed in the onshore and offshore regions, while average temperature that was by about 1.3° C warmer offshore. Food availability was an order of magnitude higher in the onshore regions compared to offshore, with the highest chl-a values recorded at 25 µg L⁻¹ (Figure 2).

Multiple environmental parameters co-varied (Figure 3a) as observed in the RDA plot at 60 m depth (Figure 3b). The first two axes of the RDA explained approximately 90% of the variation among the biological and environmental parameters. The first RDA axis was characterized by a $\Delta\Omega_{\text{cal},60}$ vertical gradient and external dissolution, with both having negative loadings along the RDA1 axis. Carapace width was negatively correlated with $\Delta\Omega_{\text{cal},60}$, whereas external dissolution was positively correlated, suggesting that larger individuals had less dissolution and were associated with lower gradients in $\Delta\Omega_{\text{cal},60}$. While OA parameters (pCO₂, pH) were all correlated as indicated by alignment with the second RDA axis, the collinearity with temperature was not significant. We found less collinearity among the environmental parameters related to the 60 m vertical gradients, such as $\Delta\Omega_{\text{cal},60}$, $\Delta\text{O}_{2,60}$, and ΔT_{60} . Here, we focused on the mechanistic drivers that are explicitly involved in the external dissolution processes, we have examined $\Delta\Omega_{\text{cal},60}$ in how it relates to external dissolution. Similarly, internal dissolution was negatively correlated with pCO₂ along the second axis with slightly higher loading along the RDA1, and also slightly negatively related with increased temperature. The implications of this association and how they related to model output (Figure 7) will be explained below.

Megalopae carapace dissolution and reduced width as responses to variable OA parameters across vertical scales

Dissolution assessment on the external surface of the exocuticle and internal surface of the endocuticle of the megalopa's carapace and pereopod exoskeleton, was conducted only after confirming that sample preservation did not impact dissolution patterns, i.e. samples preserved in ethanol vs. flash frozen did not exhibit any significant difference in their dissolution features. Using a novel categorization scheme to semi-quantify dissolution features, including ridging

structures, dissolved areas around neuritic canals, and exposed calcite crystals (Figures 4, S1 and S2; Table S2), the individuals demonstrated various extents of these features present on the external side of the carapace and the pereopod exoskeleton (Figure S2 and S3). On the carapace, the front and outer surfaces were the most affected (Figures 4 and S3). On the pereopod exoskeleton, the thoracic segments and chelae had the most severe dissolution, while the distant parts were less affected (Figure S3). On all of the examined individuals with external dissolution, we also found evidence for internal endocuticle dissolution, which was, on average, approximately half that observed on the external exocuticle surface.

Average dissolution on the exocuticle showed the strongest linear dependence with $\Delta\Omega_{\text{cal},60}$ (Figure 5; $R^2 = 0.866$, $p < 0.001$), demonstrating that the habitats with the steepest 60 m vertical gradients results in the most damaged organisms. Because of the topographic features, there is a spatial variability related to the occurrence of the steepest $\Delta\Omega_{\text{cal},60}$ gradients, meaning that the lowest exoskeleton dissolution does not always correspond to the offshore gradients.

The internal dissolution showed the most robust evidence, though not statistically significant, of correlation with pCO_2 values (Figure 5; $R^2 = 0.406$, $p = 0.065$) and negative marginal significance with temperature ($R^2 = 0.435$, $p = 0.053$). The internal dissolution rapidly intensified beyond $\text{pCO}_2 > 500 \mu\text{atm}$ (Figure 5b), with this being a robust threshold. There was no significant correlation between internal and external dissolution (Figure 5; $p = 0.18$), suggesting decoupling of the two processes.

At sites with a small $\Delta\Omega_{\text{cal},60}$, the external surface of the carapace was characterized by predominantly smooth surfaces, the absence of dissolution, and the presence of setae (Figures 7 and S2). Ridging features were present on all examined carapaces but significantly increased at the stations with the greatest $\Delta\Omega_{\text{cal},60}$ difference (Figures 4 and 5). This presence of ridging

features co-occurred with the increased occurrence of crystal exposure, ranging from increased porosity (Stage 1) to exposed crystals (Stage 2) at the sites with lower $\Delta\Omega_{\text{cal},60}$ difference, and deeper-protruding dissolution at the sites with greater $\Delta\Omega_{\text{cal},60}$ difference (Stage 2). Using image analysis, the depth of ridging structures was estimated at approximately 2 μm , around 25% of the cuticle thickness. Given the exocuticle thickness of 2–3 μm , the dissolution extended into the endocuticle (Figure 6). The extent of dissolution on pereopod exoskeleton was comparable with the external dissolution, especially at the higher dissolution values (Figure S5; $R^2 = 0.65$; $p = 0.0047$, slope = 0.901), indicating that both features were reliable metrics for dissolution assessment.

There was a distinct pattern of severe dissolution specifically developed around the calcified neuritic canals (Figure 6). In megalopae collected at inshore stations (< 200 m bottom depth), the carapace surface around the neuritic canals was markedly dissolved (Stage 2), and mechanoreceptors were often absent. Dissolution around the neuritic canals appeared to alter the morphology of the setae (Figure 6). Setae edges were partially collapsed at the places where the mechanoreceptors are anchored in, with the initial ridging features around the canals degenerated into severely dissolved surfaces at the more intense $\Delta\Omega_{\text{cal},60}$ values (Figure 6). On the megalopae from offshore stations with a smaller $\Delta\Omega_{\text{cal},60}$ the mechanoreceptors were present with no damage around the neuritic canals and less severe dissolution. Within the region of altered setae, dissolution up to 2–3 μm around the setae (Figure S4) was accompanied by significant canal deformation. This deformation appears to destabilize the attachment of the setae anchor, resulting in the setae ‘outrooting’. In some of the calcified neuritic canals, we noted the absence of setae but have not yet quantified the frequency of this occurrence.

To examine whether external or internal dissolution affects organismal or even potentially population-level metrics, dissolution measures were compared to megalopae body parameters and abundance. Here, we made an assumption that all the larval were released at the same time to be able to compare different length parameters. We detected a significant negative correlation between external dissolution and width, as indicated by reduced individual carapace width (CW; $F = 18.61$, $R^2 = 0.823$, $p = 0.013$ for the regression of CW against external dissolution on body parts; $F = 5.3$, $R^2 = 0.57$, $p = 0.08$ for the regression of CW against all external dissolution; Figure 5d), which is particularly strong in the coastal stations. This demonstrates that external OA-related exposure can indirectly result in reduced larval width. Carapace width was strongly oriented along the first RDA axis (Figure 3), while being orthogonal to internal dissolution and directly opposed to external dissolution. The latter aligns with previous findings that internal dissolution is uncoupled from carapace width (linear model $p > 0.05$), whereas external dissolution is significantly associated with carapace width (RDA plot). Other length-related parameters (CL, R-DCS, TL) were not affected by OA parameters, demonstrating that only specific body parameters, i.e., width are affected at more severe $\Delta\Omega_{\text{cal},60}$ vertical gradients.

On the higher, population-level response, only chl-a was found to be a significant driver. Abundance was positively correlated with chl-a at 60 m depth for both onshore and offshore habitats ($R^2 = 0.327$; $p = 0.008$). None of the other environmental parameters had a significant impact. However, in shallow coastal habitats with depth < 30 m, temperature was negatively related to larval abundance (for temperature at 10 m, $R^2 = 0.241$; $p = 0.02$; $F = 6.56$), although chl-a remained the dominant driver. In addition, neither carapace dissolution nor the width was

related to larval abundance, suggesting decoupling of individual- and population-level effects of environmental conditions on larval Dungeness during the present day.

Megalopae exposure history to coastal OA conditions during the month prior to sampling

Particle back-tracking results with simulated vertical migration between the ocean surface and 60 m depth over a 30-d period from the J-SCOPE simulations showed that megalopae that were released in coastal habitats (<200 m), remained in coastal habitat for nearly a month of simulation regardless of their position in the domain (Figure 7). This retention results in extended exposure to steeper coastal vertical gradients in OA conditions (Figure 2), and consequently, more intense dissolution (Figure 5).

Discussion

To our knowledge this is the first time that OA-related dissolution of calcite structures *in situ* has been demonstrated for crustaceans. Our results indicate that it is the exposure to both parameters, $\Delta\Omega_{\text{cal},60}$ (i.e. the difference in calcite saturation depth between the surface and 60 m depth) and pCO_2 , set up by as well as prolonged (<1 month) retention in the coastal waters that characterizes the suite of *in situ* parameters determining the larval crab vulnerability. This primarily demonstrates that it is not just the mean state OA conditions, but also the vertical difference in the water column that can induce negative biological responses. Using a retrospective prediction from a regression model (Figure 5a), we estimate an 8.3% increase in the extent of external carapace dissolution over the last two decades. This post-hoc estimate was based on a ΔpH changes of 0.02 unit per decade (Carter et al., 2018), comparing current average with the extent of dissolution predicted from our regression model based on the *in situ* observations (Figure 5a with the equation in the figure content) by using the estimated pH conditions two decades prior.

This is a reasonable estimate since $\Delta\Omega_{\text{cal},60}$ is highly correlated with $\Delta\Omega_{\text{pH},60}$ ($F = 204.3$, $R^2 = 0.96$, $p < 0.001$, Figure S6).

What makes this OA-dependent dissolution of megalopae particularly relevant is that the crab samples originated in the supersaturated conditions with respect to calcite (the lowest $\Omega_{\text{calc}} = 1.41$). Since the dissolution reported in other calcifiers has been demonstrated above Ω_{ara} of 1.4–1.5 (Bednaršek and Ohman, 2015; Bednaršek et al., 2016), we conclude that exoskeleton dissolution is initiated at higher $\Delta\Omega_{\text{cal},60}$ than predicted based on thermodynamic principles alone. Furthermore, using exposure metrics based on the biogeochemical model output demonstrates that 1-month long exposure in coastal habitats with large $\Delta\Omega_{\text{cal},60}$ values can result in significantly more dissolution than predicted based on snap-shot observational data. In comparison with the chemical observations, particle tracking model output indicates prolonged severity of exposure to the coastal low OA conditions, allowing for more extensive exoskeleton dissolution and reduced larval width in those habitats. It is worth noting that dissolution could be viewed as a physiological strategy to compensate against unfavorable external conditions. Dissolution of the outer calcite layer could increase the release of the bicarbonate and hydroxyl ions, raising pH, and providing a rapid alkalization of the superficial layer (Kunkel et al., 2012). This alkaline layer could then provide an additional local protection from exposure to a large $\Delta\Omega_{\text{cal},60}$ conditions by blocking protons from continuously invading the internal fluid. However, as the larvae live in highly dynamic environments, such a layer would be continuously disrupted, explaining the high extent of external dissolution.

Dissolution as a mechanism to offset OA-related extracellular acid-base disturbance?

Species with a developed capacity for ion exchange to maintain extracellular acid-base balance, are able to compensate for the effects of exposure to high pCO_2 waters and restore extracellular

pH values optimal for physiological and biogeochemical processes (Somero, 1986). They do so via energetically expensive buffering of intra- and extracellular compartments achieved through various mechanisms, such as buffering by seawater-derived bicarbonate sources (Truchot, 1979), and increased respiratory activity to reduce CO₂ loading of the extracellular fluid and non-bicarbonate buffering (Cameron, 1985; Hans et al., 2014; Michaelidis et al., 2005).

However, the downside to the well-established extracellular acid-base control is an energetically demanding process (Hans et al., 2014; Michaelidis et al., 2005; Pane and Barry, 2007; Trigg et al., 2019). Therefore, we hypothesize that the internal carapace dissolution we observed in our study could be a part of a passive ability to buffer reductions in extracellular pH, a feature found in a variety of marine invertebrates including bivalves, echinoderms, and crustaceans (Cameron, 1985; Henry et al., 1981; Lindinger et al., 1984; Spicer and Taylor, 1987; Spicer et al., 2007). The narrow neuritic canals around the mechanoreceptors allow communication through secretion across the internal-external cuticle layers (Kunkel et al., 2012). While we currently have no information on the acid-base balance within these larval crabs under prolonged exposure to steep pCO₂ vertical gradients because no controlled experiments have been conducted, we propose future studies to examine if internal dissolution could provide some level of bicarbonate ions for buffering at comparatively low cost.

Alternative hypothesis for explaining internal dissolution might be based on the severity of external dissolution extending much deeper (Figure S4) to initiate the endocuticle dissolution. Once the dissolution of the external carapace dissolution is initiated, the mineralogical-elemental structure of the mid- and endocuticle can allow for more rapid progression. The presence of high-Mg²⁺ content in the endocuticle can cause more rapid dissolution (Andersson et al., 2008), while comparatively lower Ca²⁺ content on the outward side presumably results in a weaker

carapace (Chen et al., 2008). In addition, chitin-proteinaceous matrix, such as an amorphous crystalline layer might be present, which could importantly contribute to additional dissolution. Furthermore, while the internal solubility extent may be compensated by phosphorus, it can increase hardness, thereby preventing propagation of fractures, and Sr^{2+} because it can replace Ca^{2+} in the mineralization process (Dodd, 1964). In contrast, the observation of less internal dissolution on the endocuticle side compared to the external dissolution could be due to a difference in biomineral composition. For instance, intermixing calcite in the endocuticle with organic polymers would create a durable, protective covering, which may prevent the more soluble high-Mg calcite in the endocuticle from dissolving (Chen et al., 2008). However, we have no observations of dissolution penetration all the way from the external to the internal side, we thus propose an acid-base balance strategy to be more feasible explanation for the internal dissolution.

Potential detrimental effect associated with carapace dissolution

One of the most important findings of this study is the correlation between carapace dissolution and the reduction in larval width. This could, overtime, potentially impact population dynamics. We suggest that the dissolution-length linkage could be explained by two different hypotheses: first, pronounced dissolution under severe $\Delta\Omega_{\text{cal},60}$ vertical gradients results in dissolution rate outpacing calcification rate. In this mismatch of rates of two different processes, calcification rate cannot fully compensate for dissolution and results in overall smaller width (*'the mismatch'* hypothesis). Alternatively, there could be an energetic implication behind the dissolution-induced slowdown in width. In this form of the hypothesis, an organism expends additional

energy to increase calcification to counteract dissolution, thus resulting in an energetic trade-off that potentially compromises organismal growth (the ‘*trade-off*’ hypothesis).

Furthermore, for early Dungeness crab life stages in the near-future, the prediction of more frequent and prolonged exposures to more severe $\Delta\Omega_{\text{cal},60}$ gradients (Turi et al., 2016) could have potentially deleterious consequences in terms of behavioral and sensory impairments and chelae function. First, dissolution-affected thinner structures may become too weak to retain their integrity, particularly under more severe conditions and continuous water flow, resulting in ridged, puffed surfaces. Morphological changes may in turn negatively impact larval survival by altering swimming behaviors and competence, including the ability to regulate buoyancy, maintain vertical position, and avoid predators (Morgan, 1989; Sulkin, 1984). Similar morphological structures as those observed in our study were noted in the larval form of the European lobster (Agnalt et al., 2013), which under prolonged exposure to OA conditions led to irreparable carapace deformities, and these could lead to an increase in molt-related mortalities (Small et al., 2016). Second, dissolution on both sides of carapace and pereopod exoskeleton will inevitably limit the effectiveness of the exoskeleton in providing support for muscles contraction and defense from predators, aiding homeostatic functions, and enabling feeding functions. Third, calcified neuritic canals appear to be one of the dissolution hotspots compromising setae function. Compared with undamaged setae at undissolved surfaces (Figures 6 and S2, S3), dissolved areas may not provide sufficient structural integrity for the setae (Figure 6), potentially impairing their functionality. Given the role of setae as mechanoreceptors directly involved in supporting crustacean sensory and behavior processes, we hypothesize that the absence or damage of setae within their neuritic canals may in part provide a mechanistic understanding for potential aberrant behavioral patterns found across various crustacean species under low OA

conditions, such as slower movement, less tactile recognition, and prolonged searching time, as well as impaired swimming (Alenius and Munguia, 2012; Dissanayake and Ishimatsu, 2011) and behavioral choice (de la Haye et al., 2011). These changes can result in impaired competitiveness and altered predator-prey relationships for crabs (de la Haye et al., 2012; Dodd et al., 2015; Landes and Zimmer, 2012; Wang et al., 2018). Fourth, it is currently unknown whether external dissolution in megalopae could carry over into later life stages, including the reproductively active adult stage, and what the potential consequences may be for the population dynamics. However, reduced calcification could result in poor mineralization through the intermolt period that would be especially devastating for larval crabs because of potentially smaller sizes at maturity, as well as increased vulnerability to predation during their most sensitive molting stage.

While OA parameters largely affect observed biominerological and organismal responses, population-level responses (i.e. abundances) are driven by food availability, with a lesser role for temperature in the near-shore conditions. Although biological responses at different levels of biological organization appear to be decoupled and responded to different drivers across temporal and spatial scales that need to be taken into account to improve biological forecasts and predictions. The only driver that seem to resonate across individual and population level, at least marginally, is the temperature, which might have an opposite effect on both levels. While warmer temperature negatively affects abundances, it also reduces internal dissolution, although the latter is only a marginally significant.

To more accurately predict large-scale vulnerability, it is important to consider population connectivity, related to essential population vital rates and affected by dispersal (Lowe and Allendorf, 2010). This can be partitioned into genetic connectivity and demographic

connectivity, with our model outputs demonstrating onshore-offshore connectivity along the shelf-coastal and in the northern-southern directions. This implies prolonged exposure to less suitable habitats characterized by low $\Delta\Omega_{\text{cal},60}$ in the nearshore areas that can exacerbate negative biological effects but some of them could be counteracted by higher food availability. With respect to genetic connectivity, the status of Dungeness crab as a high gene-flow species with low genetic differentiation along the US West Coast and the lack of significant adaptation patterns (Jackson and O'Malley, 2017; Jackson et al., 2018; O'Malley et al., 2017) implies that the genetic pool that might allow for adaptation under future climate scenario will be limited. This points toward the need for more comprehensive population vulnerability assessment that can link OA vulnerability with the population genetics.

Future Directions

Like dissolution in pteropods, larval dissolution observed in Dungeness crab is clear evidence that marine invertebrates are damaged by extended exposure to strong present-day OA-related vertical gradients in their natural environment. The unexplored aspect of OA impacts related to the damaged mechanoreceptors and potentially impaired sensory functions needs to be explored further. Namely, if the sensory functions are impaired, the transitioning from the larval to juvenile stage in their coastal habitat might be compromised under predicted scenarios of steeper ΔpH and $\Delta\Omega_{\text{cal},60}$ gradients (Gruber et al., 2012; Turi et al., 2016). Multiple pathways of larval vulnerability should be studied in the context of carry-over effects to the next juvenile benthic stage to explore whether crustacean molting can offset some of the detrimental effects. Such findings should be integrated into a population demographic and exposure history model that could eventually lead to improved management of Dungeness crab stocks (Fernandes et al., 2017; Lam et al., 2016).

565

566 **Acknowledgements:** We thank Carry Weekes and Anna McLasky for collecting the larval
567 individuals, Jennifer Fisher for providing guidance to Carry Weekes; Sten Littmann from Max
568 Planck Institute in Bremen, Germany for elemental analyses. We are grateful to Polona Mrak and
569 Miloš Vittori for analyses of the crab molting stages. We thank to Sandra Bigley for her editorial
570 help with the manuscript.

571 **Funding sources:** This work was supported by the NOAA's Ocean Acidification Program for
572 initial funding and NOAA Pacific Marine Environmental Laboratory (PMEL) for supporting NB,
573 RAF, SRA, and SAS. This is PMEL contribution number 4906.

574 **Competing financial interests:** There were no competing financial interests.

575

576 **References**

577 Agnalt, A.-L., Grefsrud, E. S., Farestveit, M., Larsen, M., Keulder, F. (2013). Deformities in
578 larvae and juvenile European lobster (*Homarus gammarus*) exposed to lower pH at two
579 different temperatures. *Biogeosciences*, 10, 7883–7895.

580 Akaike, H. (1973). Information theory and an extension of the maximum likelihood principle. In:
581 B. N. Petrov & F. Csaki (Eds.) Second International Symposium on Information Theory (pp.
582 267–281). Budapest, Hungary: Akademiai Kiado.

583 Alenius, B., Munguia, P. (2012). Effects of pH variability on the intertidal isopod, *Paradella*
584 *dianae*. *Marine and Freshwater Behaviour and Physiology*, 45, 245–259.

585 Andersson, A. J., Mackenzie, F. T., Bates, N. R. (2008). Life on the margin: Implications of
 586 ocean acidification on Mg-calcite, high latitude and cold-water marine calcifiers. *Marine*
 587 *Ecology Progress Series*, 373, 265–273.

588 Bednaršek, N., Feely, R. A., Reum, J. C. P., Peterson, B., Menkel, J., Alin, S. R., Hales, B.
 589 (2014). *Limacina helicina* shell dissolution as an indicator of declining habitat suitability
 590 owing to ocean acidification in the California Current Ecosystem. *Proceedings of the Royal*
 591 *Society B: Biological Sciences*, 281, 20140123.

592 Bednaršek, N., Feely, R. A., Tolimieri, N., Hermann, A. J., Siedlecki, S. A., Waldbusser, G. G.,
 593 McElhany, P., Alin, S. R., Klinger, T., Moore-Maley, B., Pörtner, H. O. (2017). Exposure
 594 history determines pteropod vulnerability to ocean acidification along the US West Coast.
 595 *Scientific Reports*, 7, 4526.

596 Bednaršek, N., Johnson, J., Feely, R. A. (2016). Comment on Peck et al: Vulnerability of
 597 pteropod (*Limacina helicina*) to ocean acidification: Shell dissolution occurs despite an
 598 intact organic layer. *Deep-Sea Research Part II: Topical Studies in Oceanography*, 127, 53–
 599 56.

600 Bednaršek, N., Ohman, M. D. (2015). Changes in pteropod distributions and shell dissolution
 601 across a frontal system in the California Current System. *Marine Ecology Progress Series*,
 602 523, 93–103.

603 Bednaršek, N., Tarling, G. A., Bakker, D. C., Fielding, S. , Cohen, A. , Kuzirian, A. , McCorkle,
 604 D. , Lézé, B., Montagna, R. (2012). Description and quantification of pteropod shell
 605 dissolution: A sensitive bioindicator of ocean acidification. *Global Change Biology*, 18,
 606 2378–2388.

607 Busch, D. S., McElhany, P. (2016). Estimates of the direct effect of seawater pH on the survival
608 rate of species groups in the California Current Ecosystem. *PLoS One*, *11*, e0160669.

609 Cameron, J. N. (1985). Compensation of hypercapnic acidosis in the aquatic blue crab,
610 *Callinectes sapidus*: the predominance of external sea water over carapace carbonate as the
611 proton sink. *Journal of Experimental Biology*, *114*, 197–206.

612 Carter, B. R., Feely, R. A., Williams, N. L., Dickson, A. G., Fong, M. B., Takeshita, Y. (2018).
613 Updated methods for global locally interpolated estimation of alkalinity, pH, and nitrate.
614 *Limnology and Oceanography Methods*, *16*(2), 119–131.

615 Chavez, F., Pennington, J. T., Michisaki, R. P., Blum, M., Chavez, G. M., Friederich, J., Messié,
616 M. (2017). Climate variability and change: Response of a coastal ocean ecosystem.
617 *Oceanography*, *30*, 128–145.

618 Chen, P.-Y., Lin, A. Y.-M., McKittrick, J., Meyers, M. A. (2008). Structure and mechanical
619 properties of crab exoskeletons. *Acta Biomaterialia*, *4*, 587–596.

620 Davis, S., Sylvia, G., Yochum, N., Cusack, C. (2017). Oregon Dungeness Crab Fishery
621 Bioeconomic Model: A Fishery Interactive Simulator Learning Tool. Version 5.7. Prepared
622 by Coastal Oregon Marine Experiment Station, Oregon State University and The Research
623 Group, LLC for the Oregon Dungeness Crab Commission.

624 de la Haye, K. L., Spicer, J. I., Widdicombe, S., Briffa, M. (2011). Reduced sea water pH
625 disrupts resource assessment and decision making in the hermit crab *Pagurus bernhardus*.
626 *Animal Behaviour*, *82*, 495–501.

627 de la Haye, K. L., Spicer, J. I., Widdicombe, S., Briffa, M. (2012). Reduced pH sea water
628 disrupts chemo-responsive behaviour in an intertidal crustacean. *Journal of Experimental*
629 *Marine Biology and Ecology*, 412, 134–140.

630 Dissanayake, A., Ishimatsu, A. (2011). Synergistic effects of elevated CO₂ and temperature on
631 the metabolic scope and activity in a shallow-water coastal decapod (*Metapenaeus joyneri*;
632 Crustacea: Penaeidae). *ICES Journal of Marine Science*, 68, 1147–1154.

633 Dodd, J. R. (1964). Environmentally controlled variation in the shell structure of a pelecypod
634 species. *Journal of Paleontology*, 38, 1065–1071.

635 Dodd, L. F., Grabowski, J. H., Piehler, M. F., Westfield, I., Ries, J. B. (2015). Ocean
636 acidification impairs crab foraging behaviour. *Proceedings of the Royal Society B:*
637 *Biological Sciences*, 282, 20150333.

638 Fabritius, H. O., Karsten, E. S., Balasundaram, K., Hild, S., Huemer, K., Raabe, D. (2012).
639 Correlation of structure, composition and local mechanical properties in the dorsal carapace
640 of the edible crab *Cancer pagurus*. *Zeitschrift für Kristallographie*, 227(11), 766–776.

641 Feely, R. A., Alin, S., Carter, B., Bednaršek, N., Hales, B., Chan, F., ..., L. Juranek (2016).
642 Chemical and biological impacts of ocean acidification along the west coast of North
643 America. *Estuarine, Coastal and Shelf Science*, 183, 260–270.

644 Feely, R. A., Okazaki, R. R., Cai, W.-J., Bednaršek, N., Alin, S. R., Byrne, R. H., Fassbender, A.
645 (2018). The combined effects of acidification and hypoxia on pH and aragonite saturation in
646 the coastal waters of the California current ecosystem and the northern Gulf of Mexico.
647 *Continental Shelf Research*, 152, 50–60.

648 Fernandes, J. A., Papathanasopoulou, E. , Hattam, C. , Queirós, A. M., Cheung, W. W., Yool, A.,
 649 Artioli, Y. , Pope, E. C., Flynn, K. J., Merino, G. , Calosi, P. , Beaumont, N. , Austen, M. C.,
 650 Widdicombe, S., Barange, M. (2017). Estimating the ecological, economic and social
 651 impacts of ocean acidification and warming on UK fisheries. *Fish and Fisheries*, 18, 389–
 652 411.

653 Fox, J., Weisberg, S. (2011). An R Companion to Applied Regression. USA: SAGE
 654 Publications.

655 Giltz, S. M., Taylor, C.M. (2017). Reduced growth and survival in the larval Blue Crab
 656 *Callinectes sapidus* under predicted ocean acidification. *Journal of Shellfish Research*, 36,
 657 481–485.

658 González-Gordillo, J. I., Rodríguez, A., Queiroga, H. (2004). Characterization of the megalopal
 659 premoult stages of the Green crab, *Carcinus Maenas* (Decapoda, Portunidae), from
 660 laboratory culture. *Journal of Crustacean Biology*, 24, 502–510.

661 Gravinese, P. M., Enochs, I. C., Manzello, D. P., van Woesik, R. (2018). Warming and pCO₂
 662 effects on Florida stone crab larvae. *Estuarine, Coastal and Shelf Science*, 204, 193–201.

663 Gruber, N., Hauri, C., Lachkar, Z., Loher, D., Frölicher, T. L., Plattner, G.-K. (2012). Rapid
 664 progression of ocean acidification in the California Current System. *Science*, 337, 220–223.

665 Hans, S., Fehsenfeld, S., Treberg, J. R., Weihrauch, D. (2014). Acid–base regulation in the
 666 Dungeness crab (*Metacarcinus magister*). *Marine Biology*, 161, 1179–1193.

667 Henry, R. P., Kormanik, G. A., Smatresk, N. J., Cameron, J. N. (1981). The role of CaCO₃
 668 dissolution as a source of HCO₃[−] for the buffering of hypercapnic acidosis in aquatic and
 669 terrestrial decapod crustaceans. *Journal of Experimental Biology*, 94, 269–274.

670 Hobbs, R. C., Botsford, L. W., Thomas, A. (1992). Influence of hydrographic conditions and
671 wind forcing on the distribution and abundance of Dungeness crab, *Cancer magister*, larvae.
672 *Canadian Journal of Fisheries and Aquatic Sciences*, 49, 1379–1388.

673 Hodgson, E. E., Kaplan, I. C., Marshall, K. N., Leonard, J., Essington, T. E., Busch, D. S.,
674 Fulton, E. A., Harvey, C. J., Hermann, A. J., McElhany, P. (2018). Consequences of spatially
675 variable ocean acidification in the California Current: Lower pH drives strongest declines in
676 benthic species in southern regions while greatest economic impacts occur in northern
677 regions. *Ecological Modelling*, 383, 106–117.

678 Jackson, T. M., O'Malley, K. G. (2017). Comparing genetic connectivity among Dungeness crab
679 (*Cancer magister*) inhabiting Puget Sound and coastal Washington. *Marine Biology*, 164(6),
680 123.

681 Jackson, T. M., Roegner, G. C., O'Malley, K. G. (2018). Evidence for interannual variation in
682 genetic structure of Dungeness crab (*Cancer magister*) along the California Current System.
683 *Molecular Ecology*, 27(2), 352–368.

684 Kaplan, I. C., Williams, G. D., Bond, N. A., Hermann, A. J., Siedlecki, S. A. (2016). Cloudy
685 with a chance of sardines: Forecasting sardine distributions using regional climate models.
686 *Fisheries Oceanography*, 25, 15–27.

687 Kunkel, J. G., Nagel, W., Jercinovic, M. J. (2012). Mineral fine structure of the American lobster
688 cuticle. *Journal of Shellfish Research*, 31, 515–526.

689 Lam, V. W. Y., Cheung, W. W. L., Reygondeau, G., Sumaila, U. R. (2016). Projected change in
690 global fisheries revenues under climate change. *Scientific Reports*, 6, 32607.

Landes, A., Zimmer, M. (2012). Acidification and warming affect both a calcifying predator and prey, but not their interaction. *Marine Ecology Progress Series*, 450, 1–10.

Lindinger, M. I., Lauren, D. J., McDonald, D. G. (1984). Acid-base balance in the sea mussel, *Mytilus edulis*. III. Effects of environmental hypercapnia on intra- and extracellular acid-base balance. *Marine Biology Letters*, 5, 371–381.

Long, W. C., Swiney, K. M., Foy, R. J. (2016). Effects of high $p\text{CO}_2$ on Tanner crab reproduction and early life history, Part II: Carryover effects on larvae from oogenesis and embryogenesis are stronger than direct effects. *ICES Journal of Marine Science*, 73(3), 836–848.

Lowe, W. H., Allendorf, F. W. (2010). What can genetics tell us about population connectivity?. *Molecular Ecology*, 19, 3038–3051.

Manno, C., Rumolo, P., Barra, M., d’Albero, S., Basilone, G., Genovese, S., Mazzola, S., Bonanno, A. (2019). Condition of pteropod shells near a volcanic CO_2 vent region. *Marine Environmental Research*, 143, 39–48.

Melzner, F., Gutowska, M. A., Langenbuch, M., Dupont, S., Lucassen, M., Thorndyke, M. C., Bleich, M., Pörtner, H. O. (2009). Physiological basis for high CO_2 tolerance in marine ectothermic animals: Pre-adaptation through lifestyle and ontogeny? *Biogeosciences*, 6(3), 4693–4738.

Michaelidis, B., Ouzounis, C., Paleras, A., Pörtner, H. (2005). Effects of long-term moderate hypercapnia on acid-base balance and growth rate in marine mussels *Mytilus galloprovincialis*. *Marine Ecology Progress Series*, 293, 109–118.

712 Miller, J. J., Maher, M., Bohaboy, E., Friedman, C. S., McElhany, P. (2016). Exposure to low pH
 713 reduces survival and delays development in early life stages of Dungeness crab (*Cancer*
 714 *magister*). *Marine Biology*, 163, 118.

715 Morgan, S. G. (1989). Adaptive significance of spination in estuarine crab Zoeae. *Ecology*, 70,
 716 464–482. <https://doi.org/10.2307/1937551>

717 North, E. W., Schlag, Z., Hood, R. R., Li, M., Zhong, L., Gross, T., Kennedy, V. S. (2008).
 718 Vertical swimming behavior influences the dispersal of simulated oyster larvae in a coupled
 719 particle-tracking and hydrodynamic model of Chesapeake Bay. *Marine Ecology Progress*
 720 *Series*, 359, 99–115.

721 North, E. W., Adams, E. E., Schlag, Z., Sherwood, C. R., He, R., Hyun, K. H., Socolofsky, S. A.
 722 (2011). Simulating oil droplet dispersal from the *Deepwater Horizon* spill with a Lagrangian
 723 approach. In Y. Liu, A. Macfadyen, Z. Ji, & R. H. Weisberg (Eds.), *Monitoring and*
 724 *Modeling the Deepwater Horizon Oil Spill: A Record Breaking Enterprise. Geophysical*
 725 *Monograph Series* (pp. 217–226). USA: American Geophysical Union.

726 Norton, E., Siedlecki, S.A., Kaplan, I.C., Hermann, A.J., Fisher, J., Morgan, C., Officer, S.,
 727 Saenger, C., Alin, S.A., Newton, J.A., Bednaršek, N., and Feely, R.A. (*in revision*). The
 728 importance of environmental exposure history in forecasting Dungeness crab megalopae
 729 occurrence using J-SCOPE, a high-resolution model for the US Pacific Northwest. *Frontiers*
 730 *in Marine Science*

731 Oksanen, J., Blanchet, F. G., Friendly, M., Kindt, R., Legendre, P., McGlinn, D., Wagner, H.
 732 (2019). *Vegan: Community Ecology Package*. R package version 2.5-5. Available at
 733 <https://CRAN.R-project.org/package=vegan>.

734 O'Malley, K. G., Corbett, K., Beacham, T. D., Jacobson, D. P., Jackson, T. M., Roegner, G. C.
 735 (2017). Genetic connectivity of the Dungeness crab (*Cancer magister*) across oceanographic
 736 regimes. *Journal of Shellfish Research*, 36(2), 453–465.

737 Pacific States Marine Fisheries Commission (2019). Species Report: Commercial Land Catch:
 738 Metric-Tons (mt), Revenue, and Price-per-pound (Price/lbs). Portland, OR: Pacific States
 739 Marine Fisheries Commission. Available at
 740 <https://reports.psmfc.org/pacfin/f?p=501:1:5808950816361::NO::> Accessed 3/25/2019.

741 Paganini, A. W., Miller, N. A., Stillman, J. H. (2014). Temperature and acidification variability
 742 reduce physiological performance in the intertidal zone porcelain crab *Petrolisthes cinctipes*.
 743 *Journal of Experimental Biology*, 217(22), 3974–3980.

744 Page, T. M., Worthington, S., Calosi, P., Stillman, J. H. (2016). Effects of elevated $p\text{CO}_2$ on crab
 745 survival and exoskeleton composition depend on shell function and species distribution: A
 746 comparative analysis of carapace and claw mineralogy across four porcelain crab species
 747 from different habitats. *ICES Journal of Marine Science*, 74(4), 1021–1032.

748 Pane, E., Barry, J. (2007). Extracellular acid-base regulation during short-term hypercapnia is
 749 effective in a shallow-water crab, but ineffective in a deep-sea crab. *Marine Ecology*
 750 *Progress Series*, 334, 1–9.

751 R Core Team (2019). R: A Language and Environment for Statistical Computing. R Foundation
 752 for Statistical Computing. Available at <https://www.R-project.org/>.

753 Schiffer, M., Harms, L., Pörtner, H., Mark, F., Storch, D. (2014). Pre-hatching seawater $p\text{CO}_2$
 754 affects development and survival of zoea stages of Arctic spider crab *Hyas araneus*. *Marine*
 755 *Ecology Progress Series*, 501, 127–139.

756 Schlag, Z. R., North, E. W. (2012). Lagrangian TRANSPort model (LTRANS v.2) User's Guide.
757 Cambridge, Maryland: University of Maryland Center for Environmental Science, Horn
758 Point Laboratory.

759 Shanks, A. L. (1995). Mechanisms of cross-shelf dispersal of larval invertebrates and fish. In: L.
760 R. McEdward (Ed.), *Ecology of Marine Invertebrate Larvae* (pp. 324–367). USA: CRC
761 Press.

762 Siedlecki, S. A., Kaplan, I. C., Hermann, A. J., Nguyen, T. T., Bond, N. A., Newton, J. A.,
763 Williams, G. D., Peterson, W. T., Alin, S. R., Feely, R. A. (2016). Experiments with seasonal
764 forecasts of ocean conditions for the northern region of the California Current upwelling
765 system. *Scientific Reports*, 6, 27203.

766 Sinclair, M. (1988). *Marine Populations: An Essay on Population Regulation and Speciation*.
767 Washington Sea Grant. Seattle, Washington: University of Washington Press.

768 Small, D. P., Calosi, P., Boothroyd, D., Widdicombe, S., Spicer, J. I. (2015). Stage-specific
769 changes in physiological and life-history responses to elevated temperature and pCO₂ during
770 the larval development of the European lobster *Homarus gammarus* (L.). *Physiological and*
771 *Biochemical Zoology*, 88, 494–507.

772 Small, D. P., Calosi, P., Boothroyd, D., Widdicombe, S., Spicer, J. I. (2016). The sensitivity of
773 the early benthic juvenile stage of the European lobster *Homarus gammarus* (L.) to elevated
774 pCO₂ and temperature. *Marine Biology*, 163, 53.

775 Somero, G. N. (1986). Protons, osmolytes, and fitness of internal milieu for protein function.
776 *American Journal of Physiology–Regulatory, Integrative and Comparative Physiology*, 251,
777 R197–R213.

778 Somero, G. N., Beers, J. M., Chan, F., Hill, T. M., Klinger, T., Litvin, S. Y. (2015). What
 779 changes in the carbonate system, oxygen, and temperature portend for the northeastern
 780 Pacific Ocean: A physiological perspective. *BioScience*, 66, 14–26.

781 Spicer, J. I., Taylor, A. C. (1987). Carbon dioxide transport and acid-base regulation in the blood
 782 of the beach-hopper *Orchestia gammarellus* (Pallas) (Crustacea: Amphipoda). *Ophelia*, 28,
 783 49–61.

784 Spicer, J. I., Raffo, A. (2007). Widdicombe, S., Influence of CO₂-related seawater acidification
 785 on extracellular acid–base balance in the velvet swimming crab *Necora puber*. *Marine*
 786 *Biology*, 151, 1117–1125.

787 Sulkin, S. D. (1984). Behavioral basis of depth regulation in the larvae of brachyuran crabs.
 788 *Marine Ecology Progress Series*, 15, 181–205.

789 Trigg, S. A., McElhany, P., Maher, M., Perez, D., Busch, D. S., Nichols, K. M. (1 August 2019).
 790 Uncovering mechanisms of global ocean change effects on the Dungeness crab (*Cancer*
 791 *magister*) through metabolomics analysis. *BioRxiv*, 574798.

792 Truchot, J. P. (1979). Mechanisms of the compensation of blood respiratory acid-base
 793 disturbances in the shore crab, *Carcinus maenas* (L.). *Journal of Experimental Zoology*, 210,
 794 407–416.

795 Tunnicliffe, V., Davies, K. T., Butterfield, D. A., Embley, R. W., Rose, J. M., Chadwick Jr, W.
 796 W. (2009). Survival of mussels in extremely acidic waters on a submarine volcano. *Nature*
 797 *Geoscience*, 2, 344–348.

Turi, G., Lachkar, Z., Gruber, N., Münnich, M. (2016). Climatic modulation of recent trends in ocean acidification in the California Current System. *Environmental Research Letters*, 11, 014007.

Walther, K., Anger, K., Pörtner, H. (2010). Effects of ocean acidification and warming on the larval development of the spider crab *Hyas araneus* from different latitudes (54° vs. 79°N). *Marine Ecology Progress Series*, 417, 159–170.

Wang, Y., Hu, M., Wu, F., Storch, D., Pörtner, H.-O. (2018). Elevated pCO₂ affects feeding behavior and acute physiological response of the Brown Crab *Cancer pagurus*. *Frontiers in Physiology*, 9, 1164.

Figures

Figure 1: The cross sections of the Dungeness crab megalopae. Left panel (a): cross section of carapace (with increasing numbers describing the transition from the thinner exo- (1) to thicker endo-cuticle (6). Right panel (b): distribution of various elements (C-carbon-a; N-nitrogen-b; Sr²⁺- strontium-c; Mg²⁺- magnesium-d; P-phosphor-e; S-sulphur-f; K-potassium-g, Ca²⁺-

calcium-h). The more intense colors depict higher elemental concentration. Spectrum
and % content of selected elements in either carapace or pereopod exoskeleton (*a*). The
numbers in (*a*) coincide with the numbers in (*b*) that indicate the position within the carapace.

Figure 2: Interpolated $p\text{CO}_{2,60}$ (*a*), $\Delta\Omega_{\text{cal},60}$ (*b*) and chlorophyll (*c*) conditions in the onshore and
offshore habitats along the US West Coast in June 2016. $p\text{CO}_2$ reflects the conditions at 60m
depth and $\Delta\Omega_{\text{cal},60}$ indicates the difference between the surface and 60 m depth. *c*) Chlorophyll
distribution and concentration (chl-a; $\mu\text{g/L}$) demonstrate an order of magnitude difference
between the regional nearshore and offshore region. The numbers indicate the stations at which
the crabs were collected.

Figure 3: Correlation matrix of environmental variables with biological endpoints for Dungeness
megalopae: (*a*) Darker green values are strong positive correlations and darker purple values are
strong negative correlations, while dimmer green and purple indicate weaker correlations; and *b*)
Redundancy analyses (RDAs) for environmental variables used in the analyses with crab
biological measurements (internal and external dissolution, carapace width).

Figure 4: External carapace and pereopod exoskeleton of the Dungeness crab megalopae (*a*) in
its undamaged form (*b*, *c*) and with dissolution presence ranging from mild (Stage 1; *d*) to severe
(Stage 2; *e*, *f*) patterns showing similarity in the structural damages (*g*) or exposed crystals (*h*).
Indicated is the scale of the measurements (μm). The undamaged megalopae originated from the
offshore or northwards habitats characterized by low $\Delta\Omega_{\text{cal},60}$ vertical gradients, while the most
severely affected megalopae came from the nearshore or coastal habitats with steep $\Delta\Omega_{\text{cal},60}$
conditions. See more detailed explanation of the exoskeleton dissolution in the Supplementary
Figures S2, S3.

Figure 5: Estimated linear relationships between ocean-acidification conditions and dissolution. Specifically for *a*) $\Delta\Omega_{\text{cal},60}$ and relative external dissolution ($R^2 = 0.87$; $p < 0.001$) with the equation of relative external dissolution = $0.181 * \Delta\Omega_{\text{cal},60} + 0.215$; *b*) Depth-integrated $\text{pCO}_{2,60}$ and relative internal dissolution ($R^2 = 0.41$; $p = 0.064$); *c*) Comparison of the relative external and internal dissolution ($R^2 = 0.24$; $p = 0.18$); and *d*) Relative external dissolution and carapace width ($R^2 = 0.57$; $p = 0.08$). Dotted lines show the linear regression fit between all points. The solid line in (*c*) is the 1:1 line and the green line in (*d*) is the regression fit only through the onshore points. See methods for explanation of the term relative dissolution. Carapace width is in mm.

Figure 6: Presence of setae on the pereopods (*a*) and carapace surface (*b*) of the megalopae on the intact individuals. The exposure to greater $\Delta\Omega_{\text{cal},60}$ differences mechanically damages the setae and results in their absence and outrooting (black squares) because of the dissolution around the neuritic canals (*d, f*) and damage with the collapsed structure (*e*).

Figure 7: Particle initialization locations (*a*) and average backtracked locations (*b-e*) for 7, 14, 21, and 30-day simulated particles exhibiting diel vertical migration (DVM) between 0 and 60 m depths. Replicate particles ($n=100$) were initialized in the model at 51 locations representing the sampling stations for the 2016 West Coast Ocean Acidification Cruise. J-SCOPE's historical simulation of ocean conditions for 2016 was used to simulate advection of particles, and each particle exhibited vertical swimming between the ocean surface at night and a maximum daytime depth of 60 m. On a weekly basis, particle locations were averaged for all 100 particles initialized at the same station, which sometimes resulted in the average location being on land. These particles were moved to the nearest shoreline. Station color varies by transect for

863 improved resolution of dispersal patterns occurring at different latitudes. The 200 m isobath is
864 shown for reference, and land is shaded in grey.

Figure 1

[Click here to download high resolution image](#)

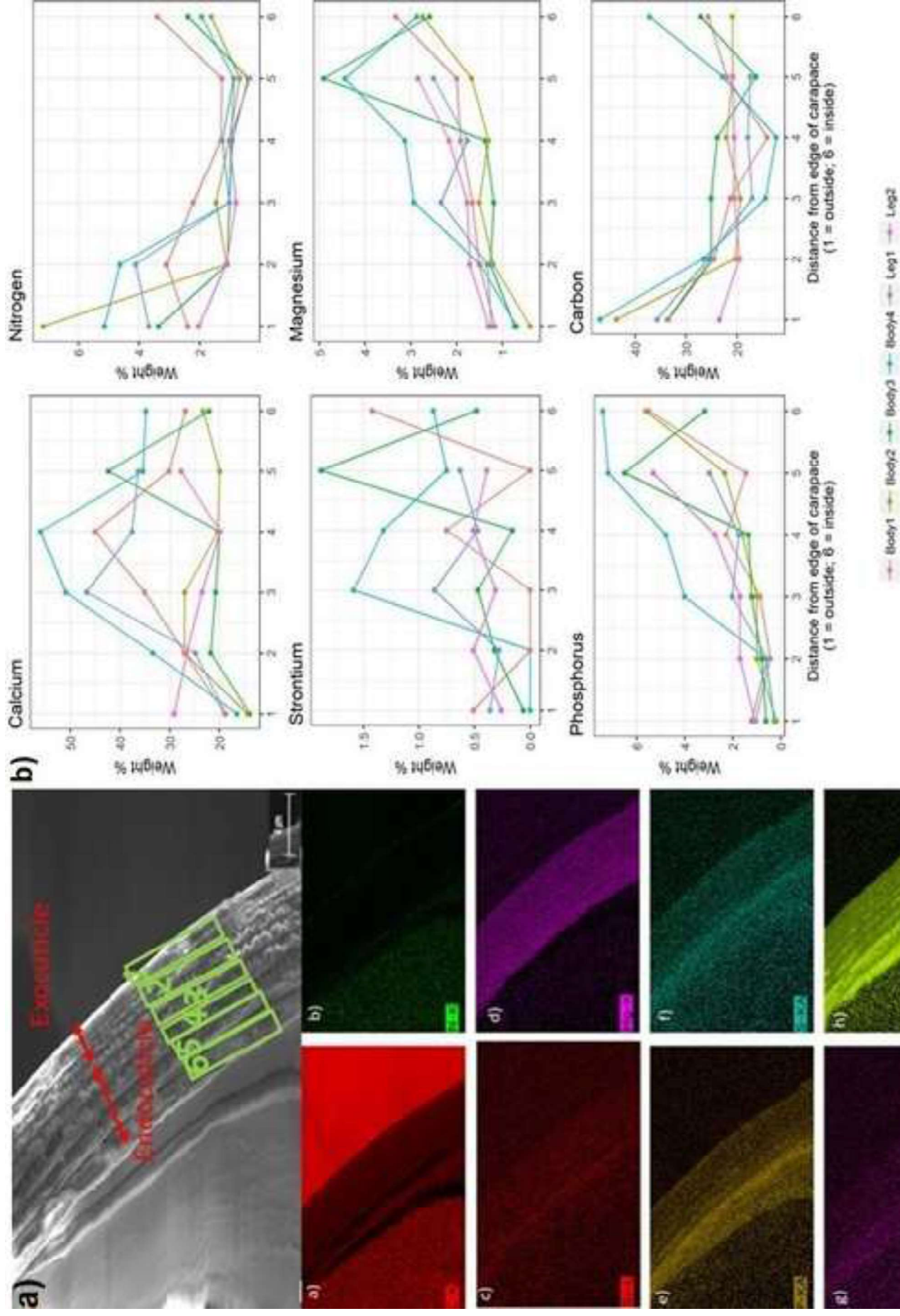


Figure 2

[Click here to download Figure: Fig2_total_final.pdf](#)

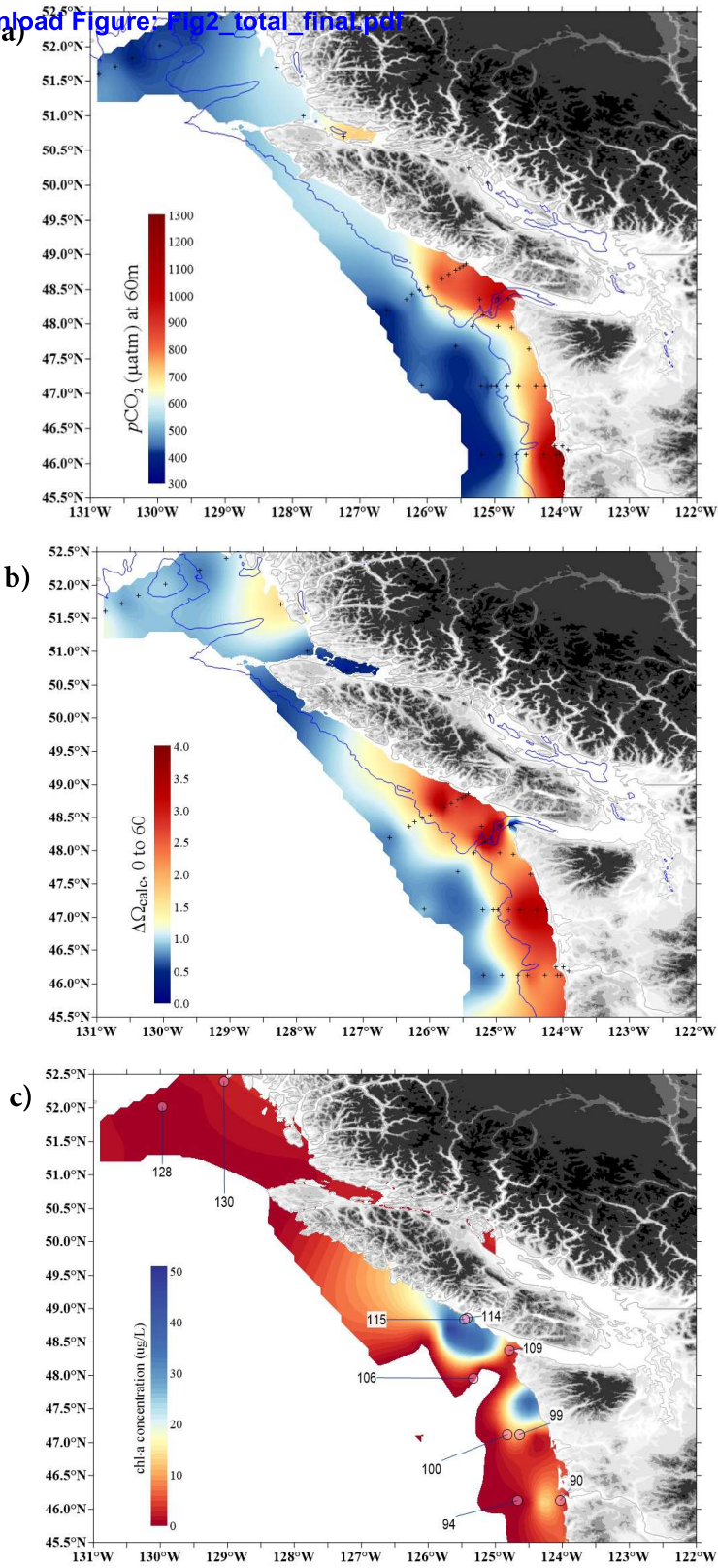


Figure 3a
[Click here to download high resolution image](#)

a)

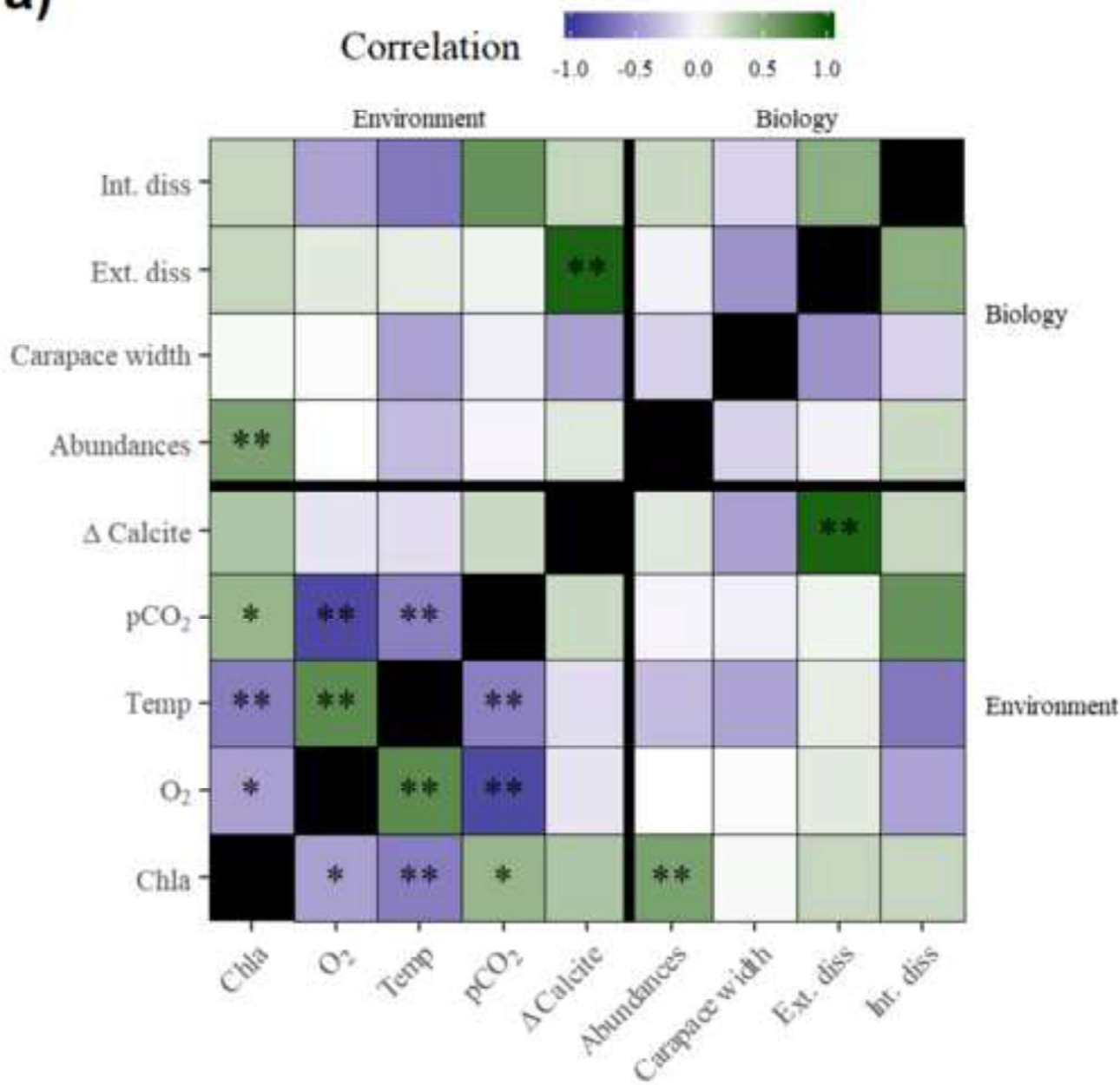


Figure 3b
[Click here to download high resolution image](#)

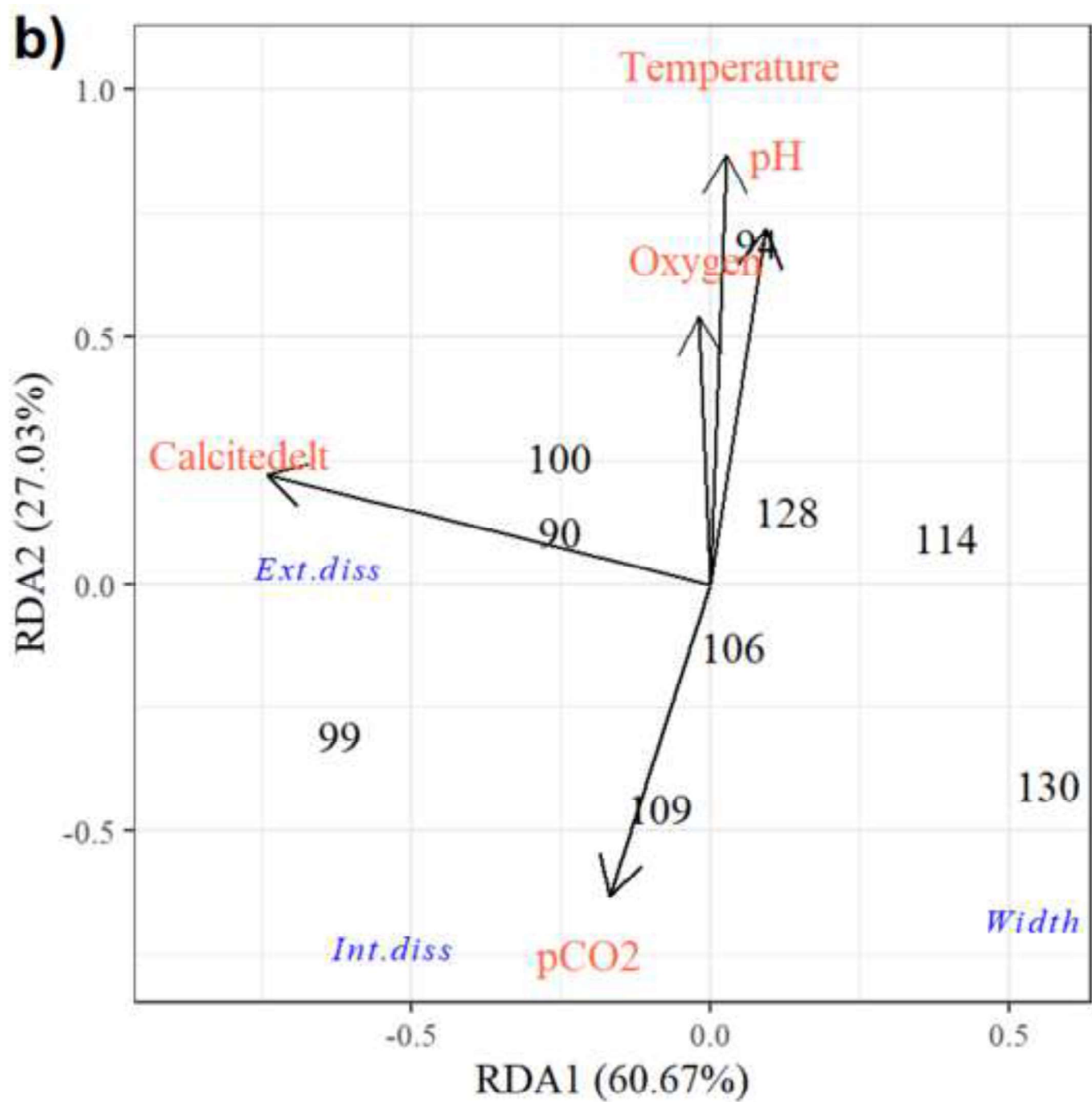


Figure 4

[Click here to download high resolution image](#)

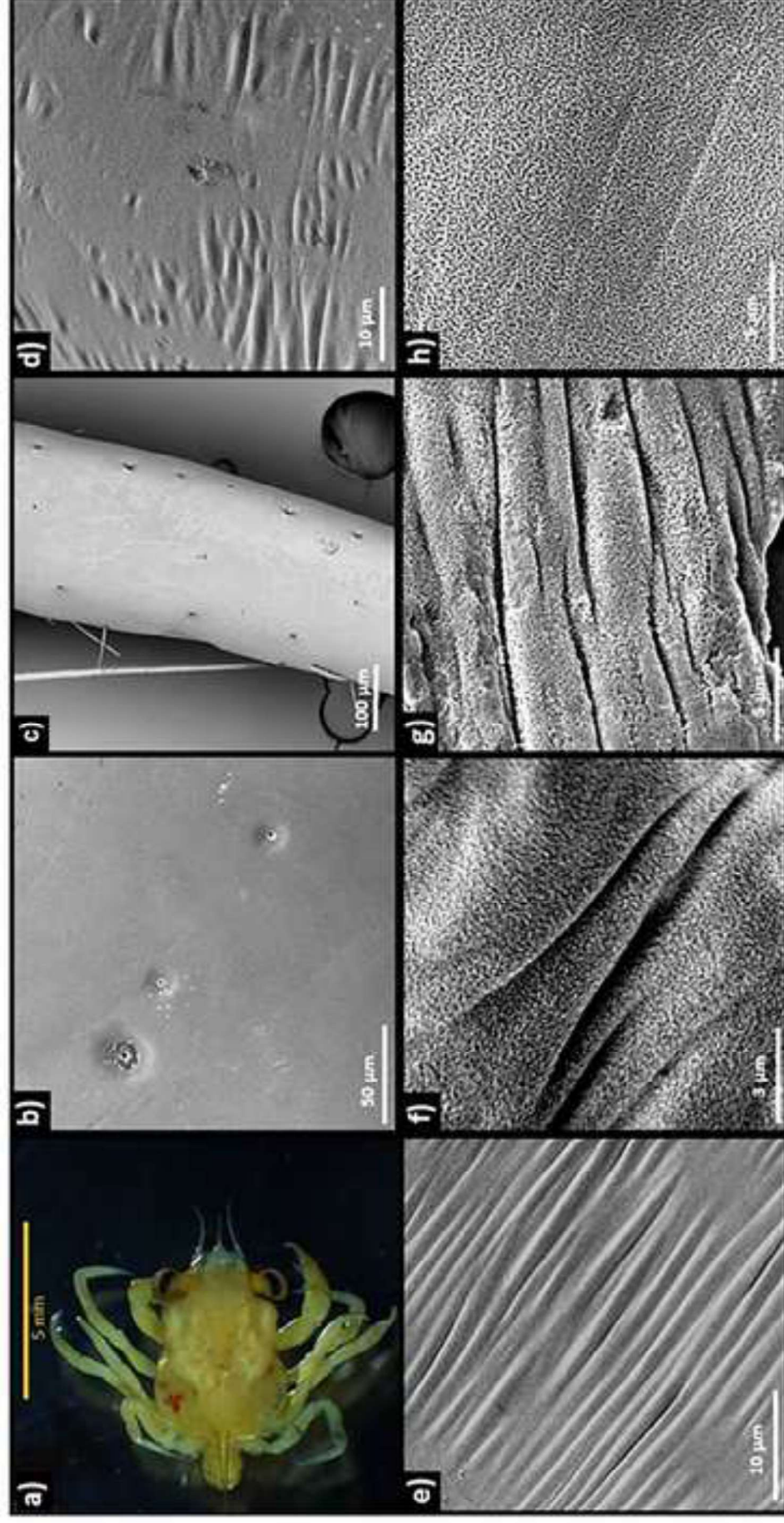


Figure 5
[Click here to download high resolution image](#)

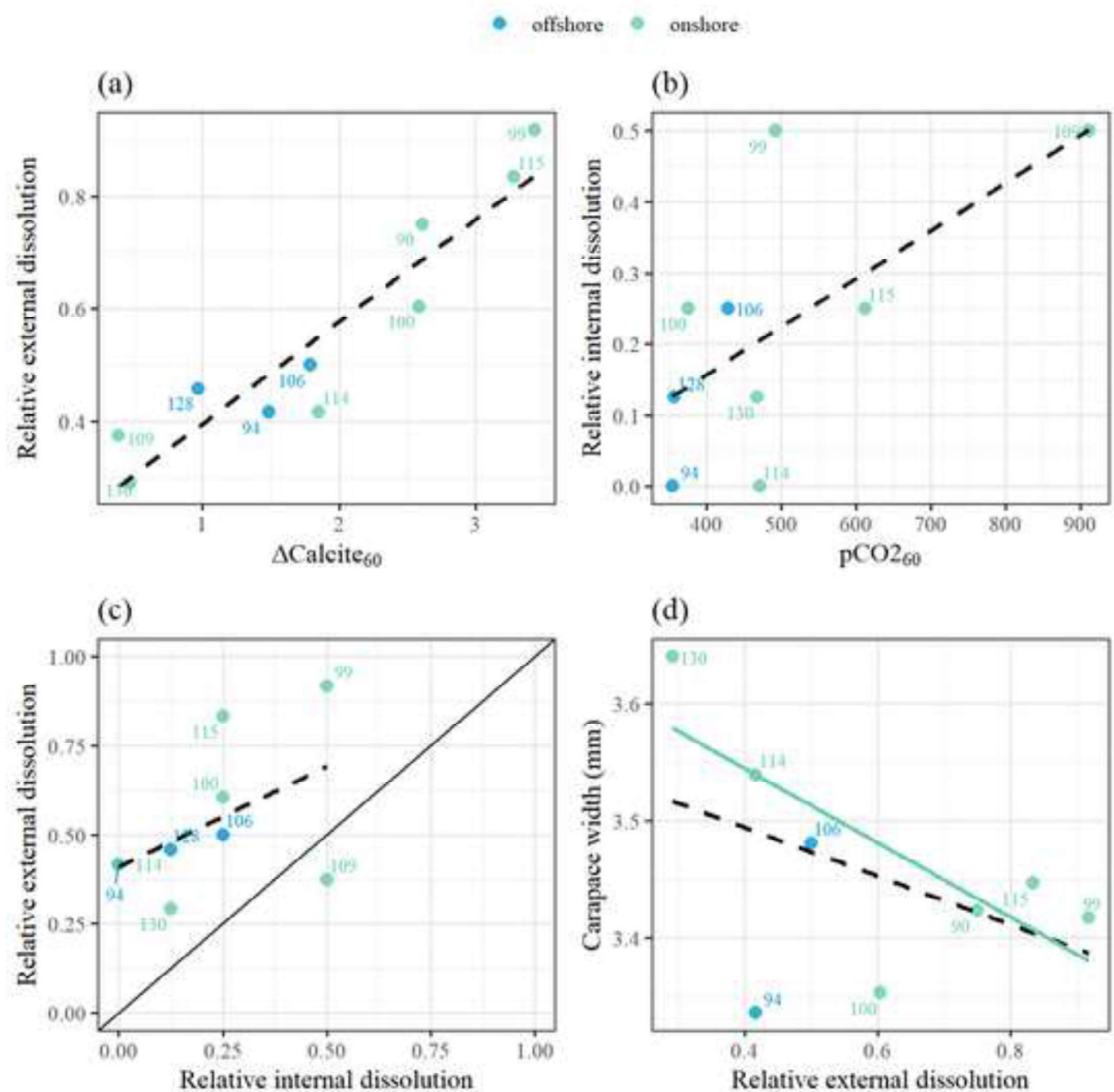


Figure 6

[Click here to download high resolution image](#)

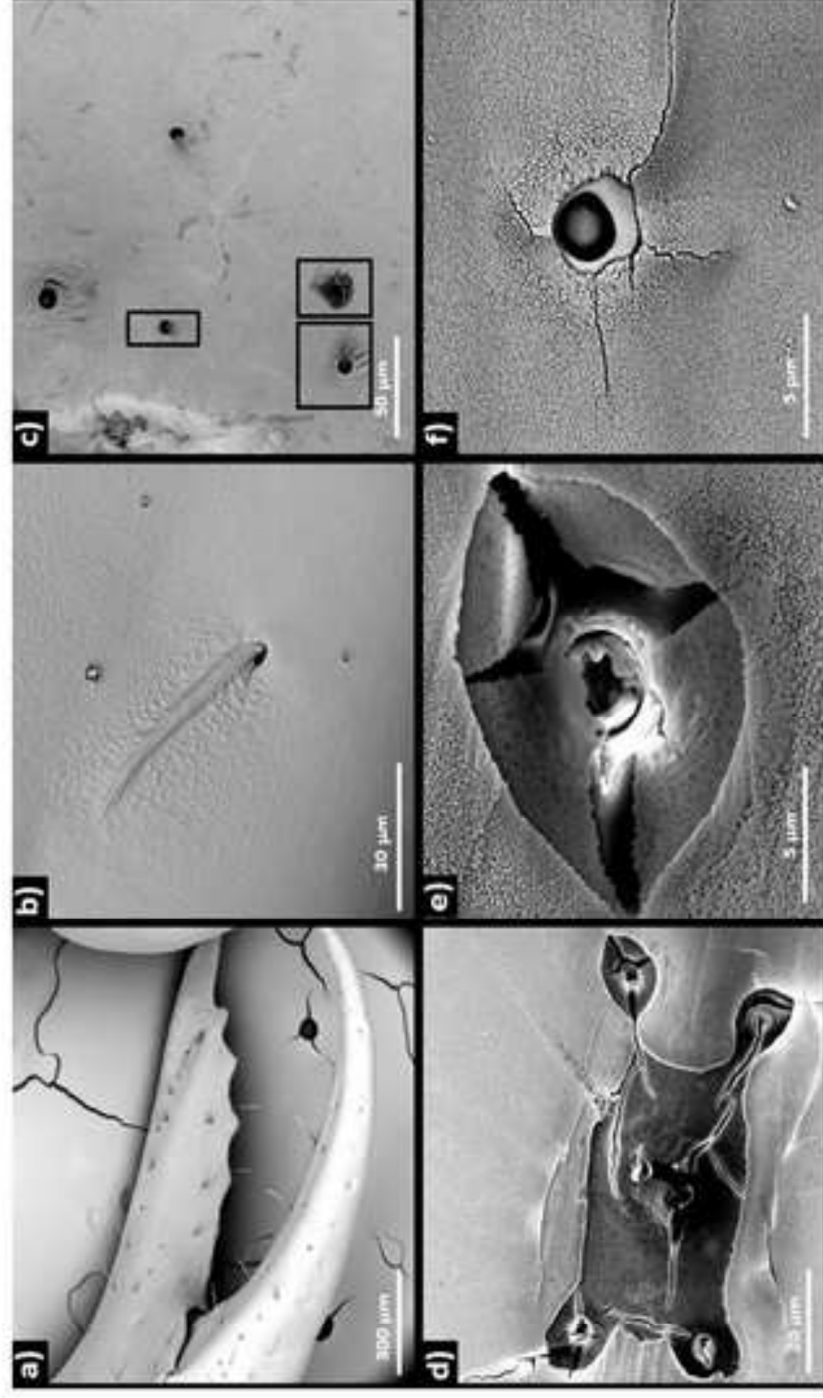


Figure 7

[Click here to download high resolution image](#)

